

Received June 18, 2020, accepted June 30, 2020, date of publication July 3, 2020, date of current version July 15, 2020.

Digital Object Identifier 10.1109/ACCESS.2020.3006795

DeepMAD: Deep Learning for Magnetic Anomaly Detection and Denoising

XIN XU^{1,2,3}, LING HUANG^{1,2}, XIAOJUN LIU^{1,2,3}, AND GUANGYOU FANG^{1,2,3}

¹Aerospace Information Research Institute, Chinese Academy of Sciences, Beijing 100190, China

²Key Laboratory of Electromagnetic Radiation and Sensing Technology, Chinese Academy of Sciences, Beijing 100190, China

³School of Electronics, Electrical, and Communication Engineering, University of Chinese Academy of Sciences, Beijing 100190, China

Corresponding author: Xin Xu (xinxu9527@yeah.net)

This work was supported in part by the National Key Research and Development Program of China under Grant 2017YFC0601803, and in part by the 13th Five-Year Equipment Advance Research Project Foundation of China under Grant JZX7Y20190253003101.

ABSTRACT In this paper we introduce an end-to-end deep learning (DL) framework for magnetic anomaly detection (MAD) and denoising. This framework consists of two neural networks: a binary classification network for magnetic anomaly detection and a regression network for geomagnetic noise suppression. The two networks work in a cascade mode: the magnetic field measurement is first sent to the detection network to check the existence of the anomaly signal, and then to the denoising network for extracting the signal from the geomagnetic noise if the detection result is positive. The core idea of our proposed method is that the characteristics of both the magnetic anomaly signal and the geomagnetic noise can be learned from massive training data. The experimental results show that: (1) under the same false alarm rate constraint, the probability of detection of our proposed method is above 80% when the signal-to-noise ratio (SNR) equals -6 dB, while the orthogonal basis function (OBF) method fails when the SNR is below 0 dB; (2) for geomagnetic noise suppression, an improvement of 10 to 15 dB is achieved for data with input SNRs between -5 and 15 dB. Our results paved the way for data-driven magnetic anomaly detection and denoising.

INDEX TERMS Magnetic anomaly detection, geomagnetic noise suppression, convolutional neural network, deep learning.

I. INTRODUCTION

Magnetic Anomaly Detection (MAD) has been one of the most important methods for detecting ferromagnetic target and is widely used in submarine detection, aeromagnetic survey, etc. For airborne MAD systems, the typical operating frequency band is 0.05Hz to 0.5Hz. Within this frequency range, there are five main sources of magnetic noise [1]: (a) Inherent sensor noise. It is the upper bound on the measurement capability and generally cannot be reduced or removed except by improving the sensor or changing to a more advanced type of sensor; (b) Platform interference noise which arises from the ferromagnetic/conducting material of the platform and its rotation in the Earth's magnetic field. This kind of noise is well modelled by the so-called Tolles-Lawson equations proposed by Leliak in 1960s and can be largely reduced by a set of sophisticated calibration procedures [2]; (c) Geomagnetic noise originated from the solar-activity induced disturbance in the Earth's magnetosphere; (d) Ocean swell

noise generated from electrical currents induced by the vertical motion of the conducting seawater, in the presence of Earth's magnetic field. It decays exponentially with altitude and can be neglected when the platform is flying relatively high [3]; (e) Geological noise which arises from the horizontal motion of MAD system across submerged concentrations of magnetic materials contained within or submerged below the seabed or ground. It can be removed by a second-pass fly or a pre-acquisition of magnetic map with high precision over the surveyed area. Since the sensitivity of advanced magnetic sensors and the performance of aeromagnetic compensation equipment have improved substantially in past decades, environmental geomagnetic noise now becomes the limiting factor of the detection range for magnetic anomaly detectors.

Many efforts have been made to improve the ability of signal detection in the presence of geomagnetic noise. The most well-known signal detection method for MAD is the Orthogonal Basis Function (OBF) matched filter [4]. The magnetic field of target, modelled as a magnetic dipole, is represented by a linear combination of three parameterized orthogonal basis functions, and then the standard matched filtering can

The associate editor coordinating the review of this manuscript and approving it for publication was Inês Domingues^{id}.

be applied for signal detection. The OBF method is theoretically optimal under the white noise assumption. However, the performance will be degraded for geomagnetic noise with a power spectrum density of $1/f^\alpha$. In [5] a whitening filter is used to flatten the noise spectrum before matched filtering. The OBF method relies on the magnetic dipole model and the straight-line moving assumption, which impose restriction on its usage. Other methods such as minimum entropy filter [6] and high order crossing method [7] are proposed. However, most of the existing magnetic anomaly signal detection methods fail when the SNR is low.

Geomagnetic noise suppression is also of great concern since important target information can be extracted from the denoised signal. The majority of existing denoising methods are based on the spatial coherence of the geomagnetic field. As early as in 1960s, coherence of geomagnetic field had been found between stations with distances up to 550 km [8]. In recent days, geomagnetic denoising experiments exploiting spatial coherence of geomagnetic field show that an SNR improvement of 10 to 20 dB can be achieved within the MAD frequency band [9]–[11]. However, real-time spatial-coherent geomagnetic noise reference data is very difficult to obtain for airborne MAD systems especially when working in the vast sea area.

Temporal coherence of geomagnetic field is implicitly exploited for the first time in [12] to enhance the ship’s ELF signal which is buried in the background noise. The noise power spectrum is iteratively updated from previous data frame when the target signal is absent and then subtracted from the current data frame. The reduction of the background noise is so substantial that the ELF radiation offers a clear means of detection. However, the assumption that data frames without targets can be found does not always hold true, which limits its application in actual scenarios.

To address the problems mentioned above, in this paper we propose an end-to-end deep learning framework for magnetic anomaly detection and denoising by exploiting both the unique signal characteristic and the temporal coherence of geomagnetic noise. This framework consists of two neural networks: a binary classification network for magnetic anomaly detection and a regression network for geomagnetic noise suppression. The two networks work in a cascade mode: the magnetic field measurement is first sent to the detection network to check the existence of the anomaly signal, and then to the denoising network for extracting the signal from the geomagnetic noise if the detection result is positive.

The paper is organized as follows. The MAD model and traditional methods are briefly introduced in Section II. Detailed description of our proposed method and network structures are given in Section III. In Section IV, the experimental setup is explained in detail. Experiment results are given in Section V, through which the comparisons

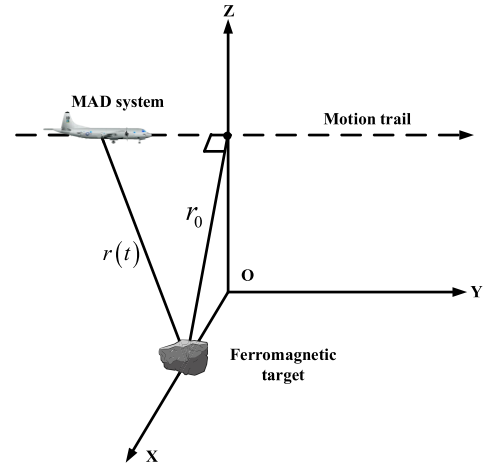


FIGURE 1. Geometry for airborne magnetic anomaly detection.

among different methods and performance analysis are made. Finally, a conclusion is drawn in Section VI.

II. PROBLEM FORMULATION

A. MAGNETIC ANOMALY DETECTION

The platform with the MAD system moves along a straight line and the ferromagnetic target of interest is assumed to be approximately static, as shown in Fig.1. The distance between sensor and target is $r(t)$, and r_0 is the shortest distance which is also known as Closest Proximity Approach (CPA). The configuration in Fig.1 is very common for most MAD applications and can be adapted to the OBF detection method which is the benchmark of our proposed method. However, our proposed method can be used in a wider range of situations.

B. ORTHOGONAL BASIS FUNCTION METHOD

The magnetic field of the target is well modelled by a magnetic dipole when $r(t)$ is large compared with target’s size. According to theory of OBF [4], the total magnetic field of the magnetic dipole can be represented by (1) if the trajectory of the relative movement between target and sensor is a straight line:

$$B_{tot} = \sum_{i=1}^3 a_i \varphi_i(\tau) \tag{1}$$

where $\tau = vt/r_0$, v is the speed of sensor platform, a_i are the coefficients and $\varphi_i(\tau)$ are the normalized orthogonal basis functions:

$$\begin{aligned} \varphi_1(\tau) &= \sqrt{\frac{24}{5\pi}} \frac{1 - \frac{5}{3}\tau^2}{(1 + \tau^2)^{2.5}} \\ \varphi_2(\tau) &= \sqrt{\frac{128}{5\pi}} \frac{\tau}{(1 + \tau^2)^{2.5}} \\ \varphi_3(\tau) &= \sqrt{\frac{128}{3\pi}} \frac{\tau^2}{(1 + \tau^2)^{2.5}} \end{aligned} \tag{2}$$

For any input signal $S(t)$ to be detected, the OBF method computes

$$T = \sum_{i=1}^3 \left| S(t)^T \varphi_i(t) \right|^2 \quad (3)$$

and compares it with a predetermined threshold value. In section V, the threshold value of the OBF method is set to be $3\sigma_T^2$ where σ_T^2 is the variance of results computed by (3) with geomagnetic noise as the input signal. Since the CPA is not known a priori, the matched filtering operation in (3) is performed in a multi-channel manner where different channels correspond to different CPA values.

The OBF method is an optimal linear signal detection algorithm for white noise in theory. The geomagnetic noise, however, is a kind of color noise with $1/f$ spectrum. The performance of OBF degrades for MAD applications. One popular solution is to place a whitening filter [5] before the OBF matched filter. The effect of whitening filter on the OBF method and our proposed method will be analyzed in section V.

C. RELATED WORKS

While the spatial coherence of geomagnetic field is well known to the MAD community, the temporal coherence receives relatively little attention. In fact, the geophysical community have been interested in the temporal statistical characterization of geomagnetic field for a long time [13]. Geomagnetic pulsation in ultra-low frequency band are divided and classified into different indexes which can be forecast for days or even months [14], [15]. Our results in section V also indicate the temporal coherence of geomagnetic noise may last for a long period of time.

Deep learning is widely used in signal detection and denoising in recent years. In speech denoising community, the 1D speech signal is transformed into the time-frequency domain to adapt the DL methods designed for image processing [16]. However, these methods are not suited for MAD processing because of the lack of information in the time-frequency domain for magnetic anomaly signal.

Signal detection and denoising of gravity wave data produced by the LIGO detector using deep learning methods are reported recently [17]. The gravity wave data are similar to the magnetic data that both of them are 1D time series which are suitable for processing in the time domain. Our proposed method in this paper differs from [17] with different network structures, more integrated processing pipeline and an emphasize on the temporal coherence of noise.

III. PROPOSED METHOD

We propose an end-to-end deep learning framework to simultaneously detect the presence of a target and extract the signal from background geomagnetic noise. As depicted in Fig.2, there are two neural networks in this framework: one is the

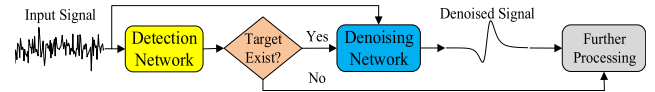


FIGURE 2. DeepMAD framework for simultaneous magnetic anomaly detection and denoising.

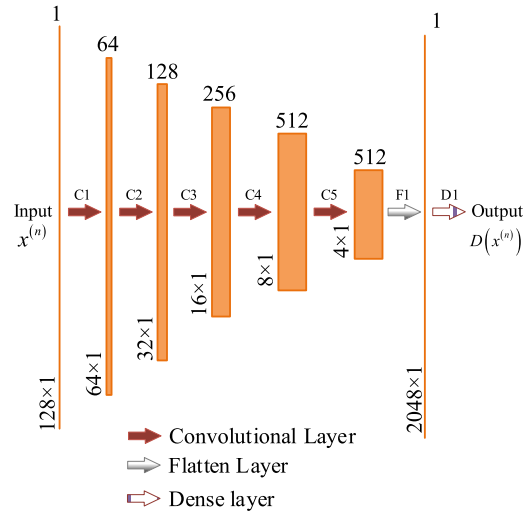


FIGURE 3. The network structure of 1D CNN for magnetic anomaly detection.

magnetic anomaly detection network, and the other is the geomagnetic denoising network. The input one-dimensional signal is first sent to the detection network, if the detection result indicates that there is a target signal buried in the noise, the original signal is sent to the denoising network to extract the clean target signal. The denoised output can be used for further processing like target localization, tracking and inversion, etc.

A. MAGNETIC ANOMALY DETECTION NETWORK

Signal detection is equivalent to binary classification in machine learning community. In [18], artificial feature extraction of magnetic anomaly signal is applied to the input data before the full connected neural network classifier. Instead, in this paper we feed the neural network classifier with original input data directly except some necessary preprocessing. By this end-to-end processing, we can make the best use of the modelling ability of neural network and massive amount of data, and more importantly the noise characteristic of geomagnetic field can be learned and utilized which will be shown in Section V.

The magnetic anomaly detection network is a deep one-dimensional (1D) CNN for binary classification, and it learns a mapping from noisy measurement vector x to signal detection result $I, D : x \rightarrow I$. The network structure is illustrated in Fig.3. The input to the network is a 128×1 vector which is the segmented measurement data of total magnetic field. There are 5 convolutional layers, 1 flatten layer and 1 output layer in the network. Different types of layers are represented by different arrows in Fig.3.

TABLE 1. Implementation details of Fig.3.

| Layer | Parameter settings |
|-------|---|
| C1 | Kernel number: 64; Kernel size: 4×1; Stride 2; Padding: “same”; Leaky Relu (slope 0.2); Dropout rate: 0.25; |
| C2 | Kernel number: 128; Kernel size: 4×1; Stride 2; Padding: “same”; Leaky Relu (slope 0.2); Dropout rate: 0.25; Batch normalization (momentum 0.8) |
| C3 | Kernel number: 256; Kernel size: 4×1; Stride 2; Padding: “same”; Leaky Relu (slope 0.2); Dropout rate: 0.25; Batch normalization (momentum 0.8) |
| C4 | Kernel number: 512; Kernel size: 4×1; Stride 2; Padding: “same”; Leaky Relu (slope 0.2); Dropout rate: 0.25; Batch normalization (momentum 0.8) |
| C5 | Kernel number: 512; Kernel size: 4×1; Stride 2; Padding: “same”; Leaky Relu (slope 0.2); Dropout rate: 0.25; Batch normalization (momentum 0.8) |
| F1 | Flatten the input to 1D vector |
| D1 | Full connection layer, activation: “sigmoid” |

The convolutional layers use a 4×1 spatial filter with stride 2 and a leaky ReLU activation function with slope 0.2. A dropout rate of 0.25 is applied for all the layers in the training phase. Batch normalization with momentum 0.8 are used in all convolutional layers except the input layer. The flatten layer transforms the input high dimensional vector to a 1D vector. The output layer is a fully connected layer with a sigmoid activation. The parameters for each layer of the detection network are listed in Table 1. The details for implementation of the network layers in this section are referred to [26].

B. GEOMAGNETIC DENOISING NETWORK

Traditional single-channel signal denoising algorithms project the noisy signal into a lower-dimensional space, then the target signal of interest is reconstructed by weighted summation of some basis functions. However, magnetic anomaly signal can hardly be denoised in this way since the parameter of OBFs cannot be precisely determined. The neural networks, known as universal function approximator, are used to solve this problem.

The first network structure used for geomagnetic noise suppression in this paper is the encoder-decoder network. Its design philosophy coincides with the above-mentioned transformation space projection method and is widely used for signal/image denoising [19]. The denoising network, as illustrated in Fig.4, learns a mapping from noisy measurement vector x to “clean” target signal y , $G : x \rightarrow y$. It consists of 5 convolutional layers and 5 deconvolutional layers. The deconvolutional layer differs from the convolutional layer that there is an additional up sampling procedure and the stride number for the convolutional kernel is 1. The parameters for each layer of the network are listed in Table 2.

Another popular network structure for regression is U-Net, which is proposed for medical image segmentation and achieves great success [20]. The original U-Net structure is modified in this paper to adapt the 1D case of our application. The network structure is almost identical with the encoder-decoder network introduced above except for the skip connections, which are copy and concatenation operations as depicted in Fig.5. Note that in [21] the

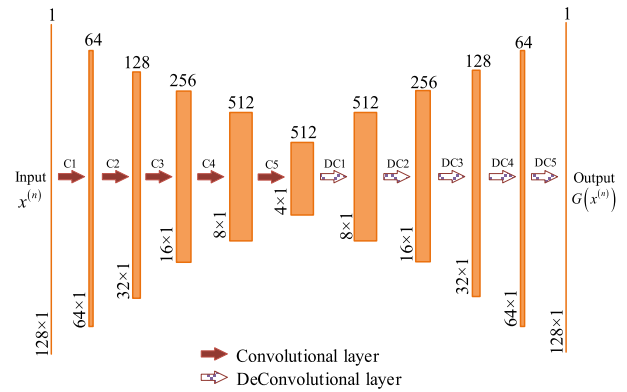


FIGURE 4. The network structure of 1D encoder-decoder for geomagnetic noise suppression.

TABLE 2. Implementation details of Fig.4 and Fig.5.

| Layer | Parameter settings |
|-------|---|
| C1 | Kernel number: 64; Kernel size: 4×1; Stride 2; Padding: “same”; Leaky Relu (slope 0.2); Dropout rate: 0.25; |
| C2 | Kernel number: 128; Kernel size: 4×1; Stride 2; Padding: “same”; Leaky Relu (slope 0.2); Dropout rate: 0.25; Batch normalization (momentum 0.8) |
| C3 | Kernel number: 256; Kernel size: 4×1; Stride 2; Padding: “same”; Leaky Relu (slope 0.2); Dropout rate: 0.25; Batch normalization (momentum 0.8) |
| C4 | Kernel number: 512; Kernel size: 4×1; Stride 2; Padding: “same”; Leaky Relu (slope 0.2); Dropout rate: 0.25; Batch normalization (momentum 0.8) |
| C5 | Kernel number: 512; Kernel size: 4×1; Stride 2; Padding: “same”; Leaky Relu (slope 0.2); Dropout rate: 0.25; Batch normalization (momentum 0.8) |
| DC1 | Upsampling:2; Kernel number: 512; Kernel size: 4×1; Stride 1; Padding: “same”; Leaky Relu (slope 0.2); Dropout rate: 0.25; Batch normalization (momentum 0.8) |
| DC2 | Upsampling:2; Kernel number: 256; Kernel size: 4×1; Stride 1; Padding: “same”; Leaky Relu (slope 0.2); Dropout rate: 0.25; Batch normalization (momentum 0.8) |
| DC3 | Upsampling:2; Kernel number: 128; Kernel size: 4×1; Stride 1; Padding: “same”; Leaky Relu (slope 0.2); Dropout rate: 0.25; Batch normalization (momentum 0.8) |
| DC4 | Upsampling:2; Kernel number: 64; Kernel size: 4×1; Stride 1; Padding: “same”; Leaky Relu (slope 0.2); Dropout rate: 0.25; Batch normalization (momentum 0.8) |
| DC5 | Upsampling:2; Kernel number: 1; Kernel size: 4×1; Stride 1; Padding: “same”; Tanh activation |

performance of encoder-decoder network and U-Net have already been compared for image to image translation. In this work, we compare their performances for 1D signal denoising for the first time.

IV. EXPERIMENTAL SETUP

A. OVERVIEW OF THE EXPERIMENTS

The performances of the detection and denoising networks introduced in Section III are verified by experiments. The two kinds of networks are trained separately using different datasets. In the training phase, the loss functions are minimized by the optimization algorithm to get optimal estimates of the parameters of the networks. In the testing phase, the samples for testing are fed to the networks to make predictions. The performance metrics, such as probability of detection (PD) and signal to noise ratio (SNR) are calculated for further analysis. The complete processes of the experiments are shown in Fig.6.

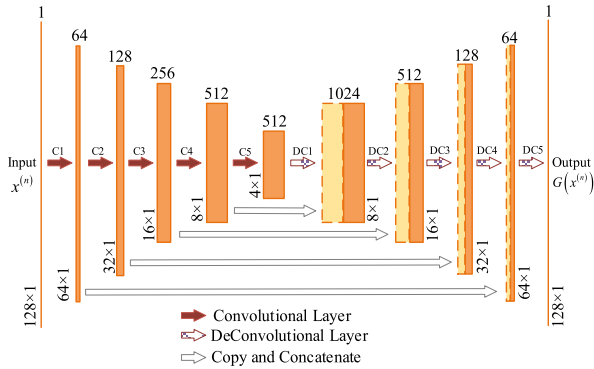


FIGURE 5. The network structure of 1D U-Net for geomagnetic noise suppression.

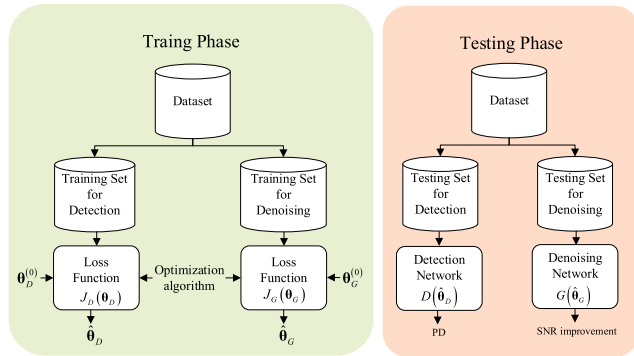


FIGURE 6. Training and testing processes of the experiments.

B. DATA PREPARATION

The data used in this paper are obtained by simulation modelling and experimental measurement.

1) MAGNETIC ANOMALY SIGNAL

The magnetic anomaly signal is simulated based on the scenario depicted in Fig.1. Although there are mathematically rigorous methods, like integral equation and method of moment, can be used for precise modelling of magnetic anomaly field, the magnetic dipole model is chosen in this paper for its simplicity and validity especially when the distance is greater than 3 times of the target size. The vector field \mathbf{B} and scalar field B_{total} of magnetic dipole are expressed as follows:

$$\mathbf{B}(\mathbf{m}, \mathbf{r}) = \frac{\mu_0}{4\pi r^3} [3r^{-2}(\mathbf{m} \cdot \mathbf{r})\mathbf{r} - \mathbf{m}] \quad (4)$$

$$B_{total}(\mathbf{m}, \mathbf{r}, \mathbf{u}_{earth}) = \mathbf{B}(\mathbf{m}, \mathbf{r}) \cdot \mathbf{u}_{earth} \quad (5)$$

where \mathbf{m} and \mathbf{r} are the magnetic moment and distance vector, respectively, $r = |\mathbf{r}|$, and \mathbf{u}_{earth} is the normalized geomagnetic field direction vector. The simulation of magnetic anomaly signal is controlled by several parameters: the CPA r_0 , the speed v , the magnetic moment \mathbf{m} and the geomagnetic direction vector \mathbf{u}_{earth} . For simplicity and without loss of generality, we fix the values of some unimportant parameters and limit the values of others to a certain range. The settings for simulation parameters are listed in Table 3.

TABLE 3. Parameters used for signal simulation.

| Parameters | Value | |
|-------------------------------|---|--------|
| Speed v (km/h) | 240 | |
| \mathbf{u}_{earth} | (-0.025, 0.735, -0.677) | |
| magnetic moment \mathbf{m} | Horizontal component (Am ²) | 100000 |
| | Vertical component (Am ²) | 300000 |
| Horizontal direction (degree) | [0,360] | |
| CPA r_0 (m) | [300,1000] | |

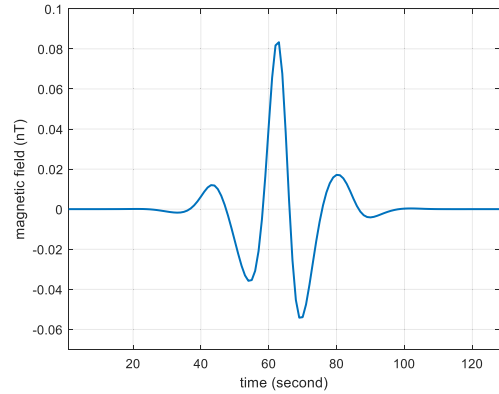


FIGURE 7. Simulated magnetic anomaly signal using dipole model.

The magnetic anomaly signals are generated using (4), (5) and Table 3. The values of parameters like horizontal direction and CPA are uniformly and randomly sampled in the predetermined intervals. The data length for each simulated signal is 128 seconds. Fig.7 is a typical signal waveform plot. The sampling frequency is set to be 1 Hz in accordance with the data rate of geomagnetic noise measurement.

2) GEOMANETIC NOISE

The geomagnetic noise data are downloaded from the INTERMAGNET website which is a global geomagnetic observatory network that provides data for scientific research [22]. The measurements are made in the station of Cocos-Keeling Islands (CKI), Western Australia. The instrument used for scalar magnetic field measurement is the GSM90 overhauser magnetometer produced by the GEM Systems. A piece of geomagnetic data with a sampling rate of 1Hz and its power spectrum density are plotted in Fig.8 and Fig.9, respectively. The data of the CKI station from January 1, 2019 to December 31, 2019 are downloaded to construct the data set.

3) DATA PREPROCESSING

The downloaded geomagnetic noise time series data are divided into 128-second segments without overlapping. A total of 243154 pieces of noise segments are obtained after discarding those with outliers or interferences. We randomly select a half of the noise samples

and add them to the simulated magnetic anomaly signal. The final dataset contains 121577 noisy samples with Geomagnetic-noise-contaminated magnetic anomaly signal and 121577 geomagnetic-noise-only samples. Bandpass filtering is applied to all the samples in the dataset with a passband from 0.05 to 0.5 Hz.

4) DATASET FOR MAGNETIC ANOMALY DETECTION

The first 120000 samples in the dataset are used for training the magnetic anomaly detection network. Since our samples are indexed in the time order of geomagnetic noise, the first 120000 samples correspond to the geomagnetic data in the first 6 months. The 7th month data, or samples index from 120001 to 140000, are used for testing the detection network. In Section V.A, the 12th month data are also used for testing to find out how long the temporal coherence of geomagnetic noise might last.

5) DATASET FOR GEOMAGNETIC DENOISING

The samples with a SNR greater than -5 dB are used to construct the dataset for the denoising networks, i.e. encoder-decoder in Fig.7 and U-net in Fig.8. A total of 55000 samples are found. The first 40000 samples are used for training and the left 15000 samples are used for testing.

C. SETTINGS FOR NETWORK TRAINING

1) LOSS FUNCTIONS

The binary cross entropy $J_D(\theta)$ and the mean squared error $J_G(\theta)$ are used as the loss functions for the detection network and denoising network, respectively.

$$J_D(\theta) = -\frac{1}{N} \sum_n \left[I^{(n)} \ln D(\mathbf{x}^{(n)}; \theta) + (1 - I^{(n)}) \ln (1 - D(\mathbf{x}^{(n)}; \theta)) \right] \quad (6)$$

$$J_G(\theta) = -\frac{1}{N} \sum_n \|\mathbf{y}^{(n)} - G(\mathbf{x}^{(n)}; \theta)\|_2^2 \quad (7)$$

where $D(\cdot)$ and $G(\cdot)$ are nonlinear functions representing the detection network and denoising network, respectively, θ is the parameters of each layer, $\mathbf{x}^{(n)}$ is the input signal to be detected or denoised, $I^{(n)}$ is 0 or 1 which indicates whether there is an anomaly signal in $\mathbf{x}^{(n)}$, $\mathbf{y}^{(n)}$ is the output of the denoising network.

2) PARAMETER INITIALIZATION

The parameters θ , including weights and biases in each network layer, should be initialized properly to accelerate the optimization procedure. The Glorot's method [24] is used to initialize the weights:

$$W \sim U \left[-\frac{\sqrt{6}}{\sqrt{n_j + n_{j+1}}}, \frac{\sqrt{6}}{\sqrt{n_j + n_{j+1}}} \right] \quad (8)$$

where $U[\cdot]$ is the uniform distribution, n_j and n_{j+1} are the number of connections in the j th and the $j+1$ th layer, respectively. The biases in all the layers are initialized to be 0.

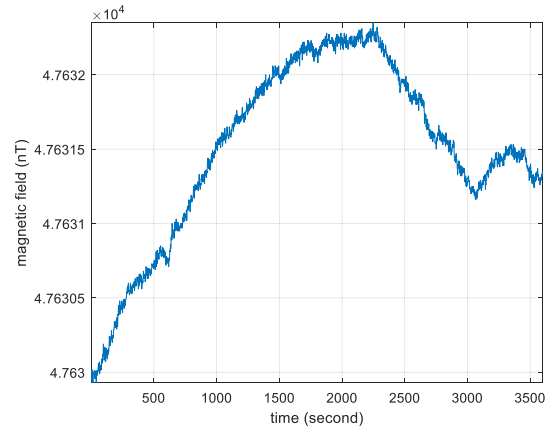


FIGURE 8. Temporal plot geomagnetic field measurements.

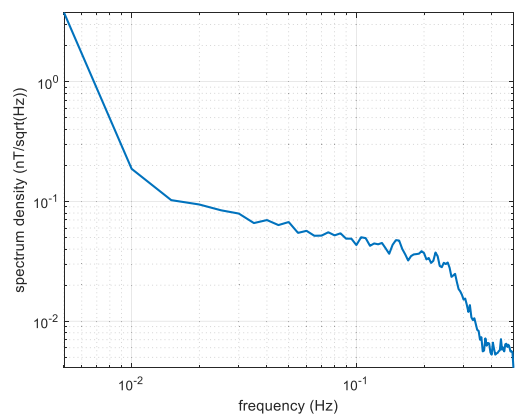


FIGURE 9. Spectrum density of geomagnetic field measurements.

3) OPTIMIZATION ALGORITHM

The RMSProp algorithm, which stands for root mean squared prop, is an adaptive learning rate optimization algorithm designed for neural networks [25]. The main operations in each iteration are expressed as follows:

$$s_t \leftarrow \gamma s_{t-1} + (1 - \gamma) \mathbf{g}_t \odot \mathbf{g}_t$$

$$\theta_t \leftarrow \theta_{t-1} - \frac{\eta}{\sqrt{s_t + \varepsilon}} \odot \mathbf{g}_t \quad (9)$$

where s_t is a state variable, η is the learning rate, ε is a small number for keeping numerical stability, and \mathbf{g}_t is the mini-batch gradient in step t .

The detection and denoising networks are trained with the RMSProp algorithm for 100 epochs with early stopping, and the mini-batch size for each epoch is 50.

D. PERFORMANCE METRICS

In order to describe the performance metrics conveniently, we introduce 4 terms about the detection result: (a) true positive (TP), which means the sample data contains a signal and is correctly classified; (b) true negative (FN), which means the sample data contains a signal and is wrongly classified; (c) false positive (TN), which means the sample data contains only geomagnetic noise and is correctly classified; (d) false

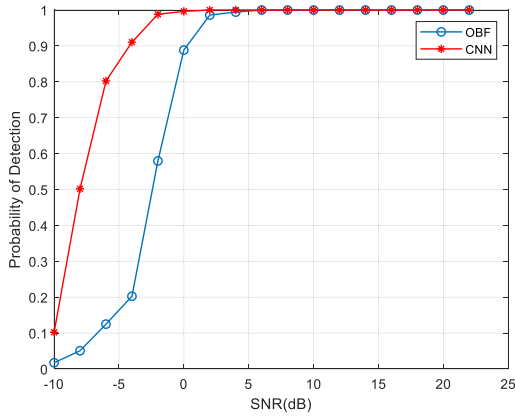


FIGURE 10. Signal detection performance comparison: CNN vs. OBF.

negative (FP), which means the sample data contains only geomagnetic noise and is wrongly classified.

The Probability of Detection (PD) is used for performance assessment of signal detection:

$$PD = \frac{\text{number of TPs}}{\text{number of TPs} + \text{number of FNs}} \quad (10)$$

In order to make comparisons between different signal detection methods, the Probability of False Alarm (PFA) rate is set to be a fixed value throughout the experiment. The PFA is defined as follows:

$$PFA = \frac{\text{number of FPs}}{\text{number of FPs} + \text{number of TNs}} \quad (11)$$

The SNR improvement is used for performance assessment of geomagnetic noise suppression:

$$SNR_{improvement} = SNR_{after} - SNR_{before} \quad (12)$$

where SNR_{before} and SNR_{after} are the SNRs of input and output data of the denoising network, respectively.

V. EXPERIMENT RESULTS AND ANALYSIS

A. MAGNETIC ANOMALY DETECTION

We use the OBF method as the benchmark of our proposed method for magnetic anomaly detection. The first 6 months data are used for training and validating, and the 7th month data are used for testing. The detection results of the CNN and OBF are illustrated in Fig.10. For comparison purposes the PFAs are fixed to be 1% throughout the experiments. The OBF method fails when the input SNR is below 0 dB, while the CNN method still maintains a relatively high PD value even for -5 dB of SNR. This 5-dB improvement of SNR implies a 21% improvement of detection range according to the magnetic dipole model.

The OBF method is often accompanied with the whitening filter to achieve better detection results as stated in section II.B. We evaluate the effect of whitening filter on OBF and CNN methods. The input data are pre-whitened before sending to the OBF and CNN detectors for both training and testing, and the results are illustrated in Fig.11 and Fig.12,

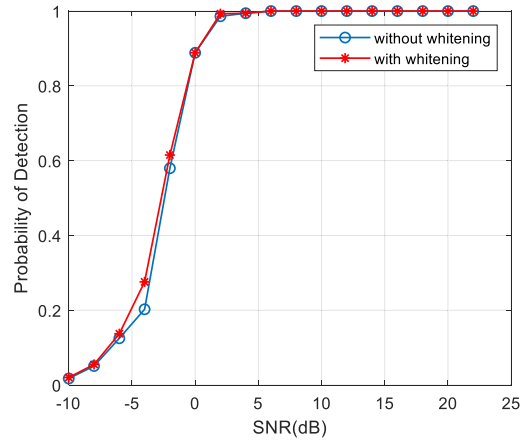


FIGURE 11. OBF signal detection performance comparison: with whitening vs. without whitening.

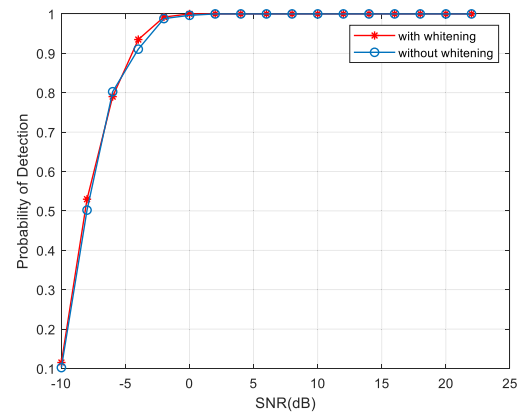


FIGURE 12. CNN signal detection performance comparison: with whitening vs. without whitening.

respectively. No significant performance improvements are found in either methods. Note that in order to keep the PFA fixed, we use different threshold values from that of Fig.10. The whitening operation tends to decrease the noise variance and thus a smaller threshold value is used.

As mentioned before, we argue that the DeepMAD framework can learn and utilize the characteristics of geomagnetic noise. Experiments are conducted to support our assumptions. We substitute the geomagnetic noise used in training/validating with gaussian white noise of the same variance. The other settings and data for testing are kept the same. The detection results are illustrated in Fig.13. The PD value is significantly lower when training with gaussian white noise especially for input SNR below 0 dB. This result shows the proposed method can indeed distinguish the geomagnetic noise and other noises. Besides, the PD performance of CNN trained with gaussian white noise is still better than that of the OBF method shown in Fig.11, which indicates the CNN method makes better use of the anomaly signal feature than that of the OBF method. The reason is that the magnetic dipole model is a nonlinear function about the magnetic moment, position, and other parameters, although the OBF method is optimal among all linear methods, the CNN method

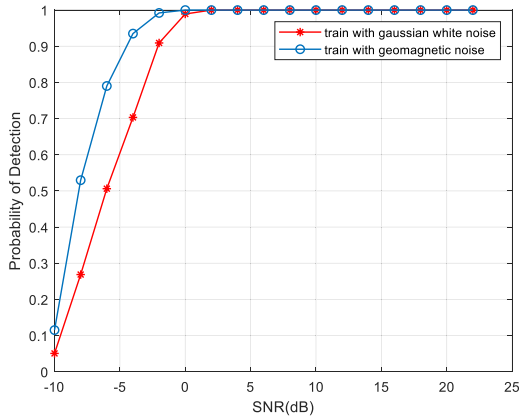


FIGURE 13. CNN signal detection performance comparison: train with geomagnetic noise vs. Gaussian white noise.

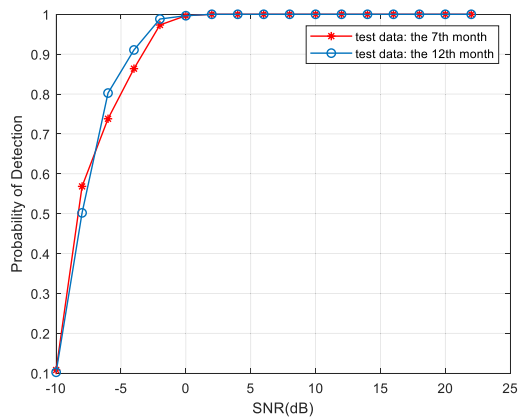


FIGURE 14. CNN signal detection performance comparison: test with the 7th month data vs. the 12th month data.

is a nonlinear method which has more powerful modelling ability.

The persistence of the temporal coherence of geomagnetic noise is also of interest to us. We use the 12th month of data for testing instead of the 7th month data while keeping all the other settings the same. The detection result is shown in Fig. 14. The PD performance remains almost unchanged. This result is so inspiring that the pre-acquisition of geomagnetic background noise may be useful for more than half a year. This is of great significance for practical MAD applications.

B. GEOMAGNETIC NOISE SUPPRESSION

Now we analyze the noise suppression performance of the denoising networks. The input data with SNR above -5 dB are used for training and testing the denoising network. The statistics of SNR improvement are calculated for different input SNR levels, as depicted in Fig. 15. For data with input SNR below 15 dB, an SNR improvement of 10 to 15 dB is achieved for both the encoder-decoder network and the U-Net. This performance is comparable to that of the far reference method which uses an additional reference sensor [9]–[11]. Fig. 15 also shows that the performance of the encoder-decoder network is slightly better than that of the

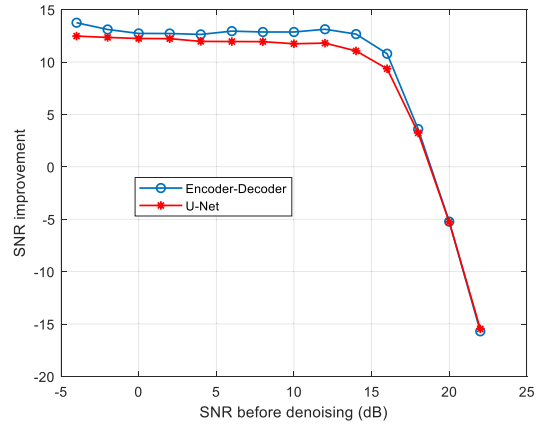


FIGURE 15. Noise suppression performance comparison: encoder-decoder network vs. U-Net.

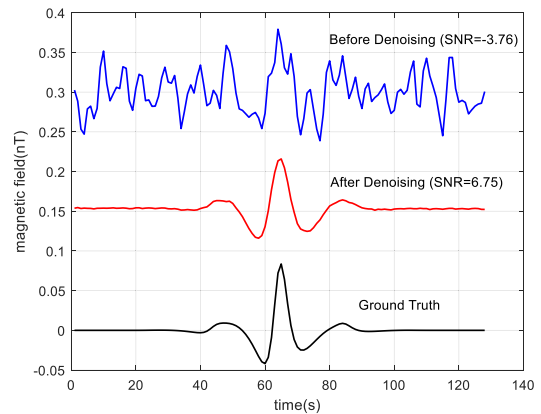


FIGURE 16. Noise suppression result for data with low input SNR.

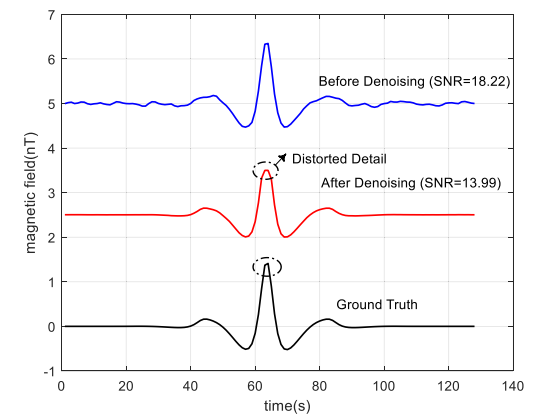


FIGURE 17. Noise suppression result for data with high input SNR.

U-Net. Although the skip connections used in U-Net have achieved great success for image segmentation, it seems to deteriorate the denoising performance in our application.

An illustration of denoising result is shown in Fig. 16. The SNR of input data is -3.76 dB and the target signal can hardly be seen from the plot. After the input data passes through the denoising network, the SNR increases to 6.75 dB and the

denoised signal can be found easily which is almost a clean copy of the ground truth.

However, from Fig.15 we also find that for data with input SNR above 15 dB, the SNR improvement decreases dramatically to nearly -20 dB. This phenomenon can be explained with Fig.17. The input and output SNRs of the data are 18.22 dB and 13.99 dB, respectively, and the SNR improvement is -4.23 dB. The reason is that compared with the ground truth, some details are lost in the denoised signal. The distortion is relatively larger than the noise component thus the denoising seems to be a disservice. This will not be a problem for practical use since the input data is very clean and requires no further processing.

VI. CONCLUSION

We have reported DeepMAD, an end-to-end deep learning framework, to tackle the problem of magnetic anomaly detection and denoising. Our integrated MAD framework is composed of two dedicated deep CNNs, a detection network for magnetic anomaly detection and a denoising network for geomagnetic noise suppression. Both of the two above CNNs fully exploit the structure of magnetic anomaly signal and temporal coherence of geomagnetic field. As a result, the DeepMAD framework with cascaded signal detection and noise suppression procedures yields a superior performance compared with conventional MAD signal detection and denoising methods that exploit only the signal structure or noise characteristic. The performance improvements are particularly large when the SNR of input magnetic measurements is below 0 dB, as we have experimentally demonstrated. Besides, the DeepMAD framework is not restricted to the experimental scenario in this paper and can be adapted to a more general setting. Our work paved the path for data-driven magnetic signal detection and denoising with improved performance.

REFERENCES

- [1] M. L. Webb and A. C. White, "Environmental noise reduction for magnetometry," U.S. Patent 8 786 277, Jul. 22, 2014.
- [2] P. Leliak, "Identification and evaluation of magnetic-field sources of magnetic airborne detector equipped aircraft," *IRE Trans. Aeronaut. Navigat. Electron.*, vol. 8, no. 3, pp. 95–105, Sep. 1961.
- [3] J. T. Weaver, "Magnetic variations associated with ocean waves and swell," *J. Geophys. Res.*, vol. 70, no. 8, pp. 1921–1929, Apr. 1965.
- [4] A. Sheinker, L. Frumkis, B. Ginzburg, N. Salomonski, and B.-Z. Kaplan, "Magnetic anomaly detection using a three-axis magnetometer," *IEEE Trans. Magn.*, vol. 45, no. 1, pp. 160–167, Jan. 2009.
- [5] A. Sheinker, A. Shkalim, N. Salomonski, B. Ginzburg, L. Frumkis, and B.-Z. Kaplan, "Processing of a scalar magnetometer signal contaminated by $1/f^\alpha$ noise," *Sens. Actuators A, Phys.*, vol. 138, no. 1, pp. 105–111, Jul. 2007.
- [6] A. Sheinker, N. Salomonski, B. Ginzburg, L. Frumkis, and B.-Z. Kaplan, "Magnetic anomaly detection using entropy filter," *Meas. Sci. Technol.*, vol. 19, no. 4, Feb. 2008, Art. no. 045205.
- [7] A. Sheinker, B. Ginzburg, N. Salomonski, P. A. Dickstein, L. Frumkis, and B.-Z. Kaplan, "Magnetic anomaly detection using high-order crossing method," *IEEE Trans. Geosci. Remote Sens.*, vol. 50, no. 4, pp. 1095–1103, Apr. 2012.
- [8] M. J. Davidson and J. R. Heirtzler, "Spatial coherence of geomagnetic rapid variations," *J. Geophys. Res.*, vol. 73, no. 6, pp. 2143–2162, Mar. 1968.
- [9] J. B. Nelson, "Preliminary results from the Sable Island geomagnetic coherence experiment," DRDC Atlantic, Dartmouth, Canada, Tech. Rep. NS TM 2006-004, Jan. 2006.
- [10] C. E. Lucas and R. Otnes, "Noise removal using multi-channel coherence," DRDC Atlantic, Dartmouth, Canada, Tech. Rep. TM 2010-302, Dec. 2010.
- [11] D. Liu, X. Xu, C. Huang, W. Zhu, X. Liu, G. Yu, and G. Fang, "Adaptive cancellation of geomagnetic background noise for magnetic anomaly detection using coherence," *Meas. Sci. Technol.*, vol. 26, no. 1, Jan. 2015, Art. no. 015008.
- [12] B. Marius, "Vessel detection using extremely low frequency magnetic anomaly detection signal," DRDC Atlantic, Dartmouth, Canada, Tech. Rep. DRDC-RDDC-2017-N034, Nov. 2017.
- [13] M. A. Vallée, L. Newitt, I. R. Mann, M. Moussaoui, R. Dumont, and P. Keating, "The spatial and temporal characteristics of PC3 geomagnetic activity over Canada in 2000, as a guide to planning the times of aeromagnetic surveys," *Pure Appl. Geophys.*, vol. 164, no. 1, pp. 161–176, Jan. 2007.
- [14] G. Pallochchia, E. Amata, G. Consolini, M. F. Marcucci, and I. Bertello, "Geomagnetic DST index forecast based on IMF data only," *Annales Geophysicae*, vol. 24, no. 3, pp. 989–999, May 2006.
- [15] G. Gonzalez and K. Schatten, "Using geomagnetic indices to forecast the next sunspot maximum," *Sol. Phys.*, vol. 114, no. 1, pp. 189–192, 1988.
- [16] Y. Xu, J. Du, L.-R. Dai, and C.-H. Lee, "An experimental study on speech enhancement based on deep neural networks," *IEEE Signal Process. Lett.*, vol. 21, no. 1, pp. 65–68, Jan. 2014.
- [17] D. George and E. A. Huerta, "Deep learning for real-time gravitational wave detection and parameter estimation: Results with advanced LIGO data," *Phys. Lett. B*, vol. 778, pp. 64–70, Mar. 2018.
- [18] S. Liu, J. Hu, P. Li, C. Wan, Z. Chen, M. Pan, Q. Zhang, Z. Liu, S. Wang, D. Chen, J. Hu, and X. Pan, "Magnetic anomaly detection based on full connected neural network," *IEEE Access*, vol. 7, pp. 182198–182206, 2019.
- [19] P. Vincent, H. Larochelle, I. Lajoie, Y. Bengio, and P.-A. Manzagol, "Stacked denoising autoencoders: Learning useful representations in a deep network with a local denoising criterion," *J. Mach. Learn. Res.*, vol. 11, no. 12, pp. 3371–3408, Dec. 2010.
- [20] O. Ronneberger, P. Fischer, and T. Brox, "U-net: Convolutional networks for biomedical image segmentation," in *Proc. Int. Conf. Med. Image Comput. Comput.-Assist. Intervent.*, 2015, pp. 234–241.
- [21] P. Isola, J.-Y. Zhu, T. Zhou, and A. A. Efros, "Image-to-image translation with conditional adversarial networks," in *Proc. IEEE Conf. Comput. Vis. Pattern Recognit. (CVPR)*, Jul. 2017, pp. 5967–5976.
- [22] J. J. Love and A. Chulliat, "An international network of magnetic observatories," *EOS, Trans. Amer. Geophys. Union*, vol. 94, no. 42, pp. 373–374, Oct. 2013.
- [23] S. M. Kay, "Statistical decision theory I," in *Fundamentals of Statistical Signal Processing (Detection Theory)*, vol. 2, 1st ed. Englewood Cliffs, NJ, USA: Prentice-Hall, 1998.
- [24] X. Glorot and Y. Bengio, "Understanding the difficulty of training deep feedforward neural networks," in *Proc. 13th Int. Conf. Artif. Intell. Statist.*, 2010, pp. 249–256.
- [25] T. Tieleman and G. Hinton, "Lecture 6.5-RMSPROP: Divide the gradient by a running average of its recent magnitude," *COURSERA, Neural Netw. Mach. Learn.*, vol. 4, no. 2, pp. 26–31, 2012.
- [26] I. I. Goodfellow, Y. Bengio, and A. Courville, *Deep Learning*. Cambridge, MA, USA: MIT Press, 2016.



XIN XU received the B.S. degree in electrical engineering from Wuhan University, Wuhan, China, in 2008, and the M.S. degree in electrical engineering from the University of Chinese Academy of Sciences, Beijing, China, in 2011, where he is currently pursuing the Ph.D. degree. He is currently an Assistant Professor with the Key Laboratory of Electromagnetic Radiation and Sensing Technology, Institute of Electronics (IE), Chinese Academy of Sciences (CAS). His research interests include electromagnetic detection and imaging, signal processing, and machine learning.



ware development, and geophysical exploration equipment design and testing.

LING HUANG received the M.S. and Ph.D. degrees in geophysical prospecting and information technology from Jilin University, Changchun, China, in 2007 and 2010, respectively. He is currently an Associate Professor with the Key Laboratory of Electromagnetic Radiation and Sensing Technology, Institute of Electronics (IE), Chinese Academy of Sciences (CAS). He is currently focusing on geophysical electromagnetic detection method research, data processing software development, and geophysical exploration equipment design and testing.



XIAOJUN LIU received the Ph.D. degree from the Chinese Academy of Sciences (CAS), Beijing, China, in 2001. He is currently a Professor with the Institute of Electronics (IE), CAS. His research interests include instrument development, and data and image processing.



GUANGYOU FANG received the B.S. degree in electrical engineering from Hunan University, Changsha, China, in 1984, and the M.S. and Ph.D. degrees in electrical engineering from Xi'an Jiaotong University, Xi'an, China, in 1990 and 1996, respectively. From 1990 to 1999, he was an Engineer, an Associate Professor, and a Professor with the China Research Institute of Radiowave Propagation. From 2000 to 2001, he was a Visiting Scholar with the University of Trieste, Trieste, Italy, and the International Center for Science and High Technology, United Nations Industrial Development Organization, Trieste. From 2001 to 2003, he was a Special Foreign Research Fellow of the Japan Society for the Promotion of Science, working with Tohoku University, Sendai, Japan. Since 2004, he has been a Professor with the Institute of Electronics, Chinese Academy of Sciences (CAS), Beijing, China, and the Director of the Key Laboratory of Electromagnetic Radiation and Sensing Technology. Since 2019, he has also been with the Aerospace Information Research Institute, CAS. He has authored or coauthored more than 400 publications. His research interests include ultrawideband radars, ground-penetrating radar signal-processing and identification methods, terahertz imaging technology, and computational electromagnetics.

...